On the determination of epipoles using cross-ratios

Q.-T. Luong
SRI International
333 Ravenswood av.
Menlo Park, CA 94025

O.D. Faugeras
I.N.R.IA.
2004, route de Lucioles
06902 Sophia-Antipolis, France

Abstract

We study the problem of computing the position of the epipoles in a pair of uncalibrated images. The approach, which is based on the invariance of the cross-ratio by the *epipolar transformation*, exploits algebraic constraints obtained from point correspondences and provides a solution in which only the epipoles are involved. This is in opposition to the methods based on the computation of the fundamental matrix. These notions are first presented as well as the new *epipolar ordering constraint*. Three families of methods are successively considered: the first uses statistics on closed-form solutions provided by the so-called *Sturm method*, the second intersect plane cubics through deterministic procedures, and the third is based on non-linear minimizations of a difference of cross-ratios. We discuss the shortcomings of each and show, using numerous experimental comparisons, that there is a trade-off between elegance and robustness to noise. The cross-ratio based methods do not turn out to be a generally viable alternative to the method based on the fundamental matrix.

Keywords

1 Introduction

Epipolar geometry provides a constraint well-known in stereovision. A particularly interesting aspect of this constraint is that it is purely projective and therefore can be exploited with uncalibrated images. A lot of useful tasks can be performed using knowledge of the epipolar geometry: recovery of the 3D projective structure of a scene from point matches, obtention of projective invariants, prediction of image features in an image from features in two other images, synthesis of an image from several images, segmentation of rigid independent motions, and self-calibration of a moving camera. For a list of references concerning these tasks, see the conclusion of [14]. More recently, affine geometry has been found to provide an interesting framework borrowing some nice characteristics from both Euclidean geometry and projective geometry. Affine calibration also requires the determination of one epipole [15], in addition to the plane at infinity.

The established method to recover the epipolar geometry is to compute the Fundamental matrix [2, 14, 7], generalizing Longuet-Higgins' eight-point algorithm [10]. It has been shown [13] that the difficult part in the determination of the Fundamental matrix is the determination of the epipoles, in the sense that the stability of epipoles characterizes the stability of the Fundamental matrix. In addition, in some of the applications previously mentioned, one does not need to know the full Fundamental matrix (seven parameters), but only one or two epipoles (two or four parameters).

In order to investigate an alternative to methods based on the computation of the Fundamental matrix, this paper proposes some new methods, based on the invariance of the cross-ratio, to recover the epipoles directly, and gives an empirical assessment of their numerical properties.

We begin by presenting the *epipolar transformation* upon which all the methods investigated in this paper are based, as well as the *epipolar ordering constraint* which can be used to match epipoles computed separately in two images. We then investigate three families of methods. The first family, based on a closed-form solution, is elegant, but very sensitive to noise. In order to gain robustness to noise, two computationally more expensive methods are studied next, which require

iterative computations: a method which intersects plane cubics through deterministic procedures, and a method based on non-linear minimizations of a difference of cross-ratios. The results of the last one are compared to the results of the Fundamental matrix method.

2 More on epipolar geometry

When considering two projective views, the main geometric property is known in computer vision as the *epipolar constraint*. In this section, we present two lesser known consequences of this construction: the existence of a homography between sets of epipolar lines, and an ordering relation between these lines, which is a consequence of visibility.

2.1 The epipolar transformation

The classical elements of epipolar geometry are presented in the left part of figure 1. Let C be the optical center of the first camera and C' that of the second. The line $\langle C, C' \rangle$ projects to a point e in the first retinal plane $\mathcal{R}$ and e' in the second retinal plane $\mathcal{R}'$. The points e, e' are the epipoles. The lines through e in the first image and the lines through e' in the second image are the epipolar lines. The epipolar constraint is well-known in stereovision: for each point m in the first retina, projection of an object point M, the corresponding point m' lies on its epipolar line l'_m, projection of $\langle C$,M$\rangle$ in the second retina.

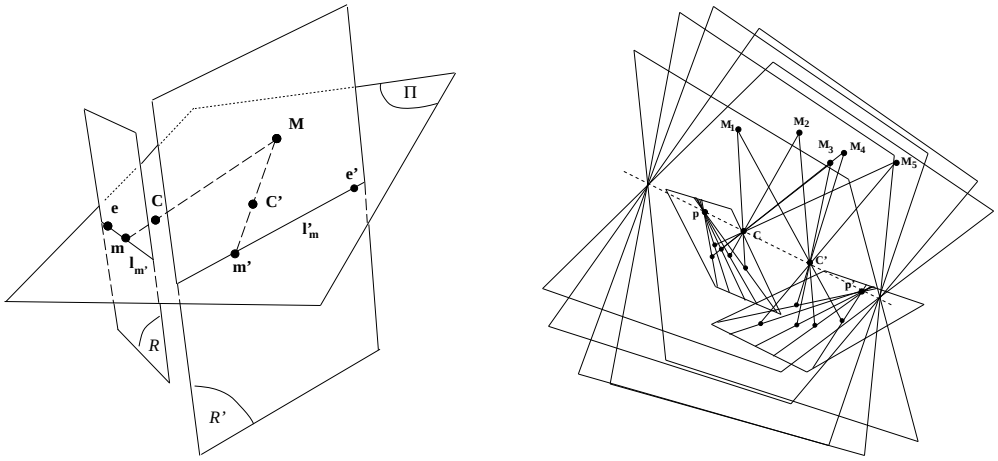

Figure 1: The epipolar geometry and epipolar pencils

Let us consider the one parameter family of planes going through $\langle C, C' \rangle$. This family is a

pencil of planes, shown on the right in Figure 1. Let Π be any plane containing $\langle C, C' \rangle$. Then Π projects to an epipolar line l in the first image and to an epipolar line l' in the second image. Since we suppose that the camera performs a projective transformation of object space into image space (a reasonable hypothesis, which amounts to neglecting lens distortion [19]), the correspondences $\Pi \mapsto l$ and $\Pi \mapsto l'$ are homographies between the two pencils of epipolar lines and the pencil of planes containing $\langle C, C' \rangle$. It follows that the correspondence $l \mapsto l'$ is a homography, called the *epipolar transformation* (see [14] for more details).

Let $m_i \leftrightarrow m'_i$, $1 \leq i \leq n$, a set of point correspondences. If the points e and e' are epipoles compatible with these correspondences, then there exists a homography that maps each of the lines $\langle e, m_i \rangle$ to the line $\langle e', m'_i \rangle$, for $1 \leq i \leq n$.

It has been shown [17] that the reciprocal is also true. The existence of such an homography is equivalent to the conservation of the cross-ratios:

$$\forall i, j, k, l \quad \{\langle \mathbf{e}, \mathbf{m}_i \rangle, \langle \mathbf{e}, \mathbf{m}_j \rangle, \langle \mathbf{e}, \mathbf{m}_k \rangle, \langle \mathbf{e}, \mathbf{m}_l \rangle\} = \{\langle \mathbf{e}', \mathbf{m}'_i \rangle, \langle \mathbf{e}', \mathbf{m}'_j \rangle, \langle \mathbf{e}', \mathbf{m}'_k \rangle, \langle \mathbf{e}', \mathbf{m}'_l \rangle\}$$

2.2 The epipolar ordering

We are going to see that knowledge of the epipoles induces an ordering relation over the set of epipolar lines. If point correspondences are considered, this ordering induces some constraints on the possible positions of the epipole.

Let us first show that:

> Each pair of corresponding epipolar lines divides the retinal plane into two corresponding half-planes.

Let l be an epipolar line of the first retinal plane $\mathcal{R}$, and l' be the corresponding epipolar line of $\mathcal{R}'$. The plane $\mathcal{R}$ is divided by l in two half-planes, $\mathcal{R}_a$ and $\mathcal{R}_b$, and the same (with primes) applies to the second image. Let m_1 and m'_1 be two corresponding points, lying respectively in the half-planes $\mathcal{R}_a$ and $\mathcal{R}'_a$ We are going to show that if m_2 is a point of $\mathcal{R}_a$, then its correspondent m'_2 must also lie in $\mathcal{R}'_a$. Let Π be the epipolar plane corresponding to the epipolar lines l and l'. It determines two half-spaces $\mathcal{E}_c$ and $\mathcal{E}_d$, and contains the optical centers C and C'. Let M_1 be the 3D point projected to m_1 and m'_1, and let M_2 be the 3D point projected to m_2 and m'_2. The points m_1 and m_2 are in the same half-space $\mathcal{E}_c$. The lines $\langle C, m_1 \rangle$ et $\langle C, m_2 \rangle$ intersect the plane

Π in C, and contain the points M_1 and M_2. Now the key point is that the cameras can observe only one half space, the other being behind them, from which we conclude that the points on these lines are ordered as Cm_1M_1 and Cm_2M_2, or m_1CM_1 and m_2CM_2. Let us consider the first case. The point C belongs to the separating plane. The points m_1 and m_2 are in the same half-space $\mathcal{E}_c$. Therefore the half-line of $\langle C, m_1\rangle$ starting at C and containing m_1 is entirely contained in the half-space $\mathcal{E}_c$, and the same can be said for the half-line of $\langle C, m_2\rangle$ starting at C and containing m_2. Since M_1 and M_2 belongs to these half-lines, they are both in the same half-space $\mathcal{E}_c$. The second case is similar. From the fact that they belong to the same half-space, it is easy to see that their projection in the second image belongs also to the same half-plane. This property is illustrated by Figure 2.

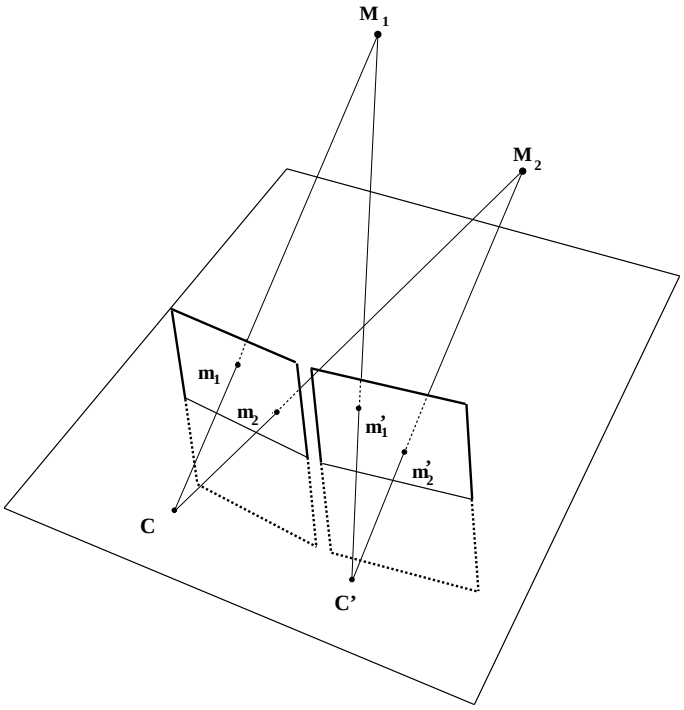

Figure 2: Pair of epipolar lines dividing the retinal planes into two corresponding half-planes.

Let us choose an orientation for each of the retinal planes. Because this orientation is arbitrary, the following exposition is unchanged if all the angles in one (or both) of the retinas are replaced by their opposites.

We can infer from the previous proposition the following property, illustrated by the top row of diagrams in Figure 3: if, in Image 1, we observe a configuration of three epipolar half-lines l_1, l_2,

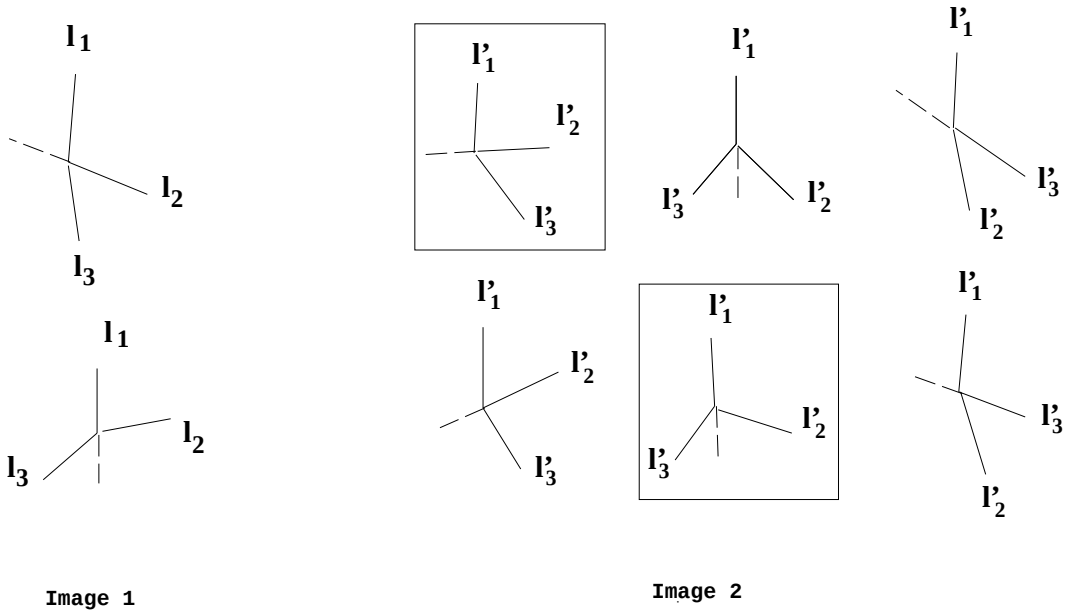

Figure 3: Compatible and incompatible configurations of epipolar lines. If the configuration of epipolar lines is as in Image 1, then the compatible configuration of epipolar lines in Image 2 is the one in the box. The other configurations are incompatible.

l_3 starting from the epipole $\mathbf{e}$ and containing the points m_1, m_2, et m_3, respectively, such that

$$0 \leq \langle \widehat{l_1, l_2} \rangle \leq \langle \widehat{l_1, l_3} \rangle \leq \pi \tag{1}$$

and if l'_1, l'_2, l'_3 are the epipolar half-lines starting from the epipole $\mathbf{e}'$ and containing the corresponding points m'_1, m'_2, m'_3 in the second image, then we must have

$$0 \leq \langle \widehat{l'_1, l'_2} \rangle \leq \langle \widehat{l'_1, l'_3} \rangle \leq \pi \tag{2}$$

Given the three epipolar half-lines l_1, l_2, l_3 verifying the constraint (1), the two only types of configurations of epipolar half-lines that can violate the constraint (2) are those for which

$$0 \leq \langle l'_1, l'_3 \rangle \leq \langle l'_1, l'_2 \rangle \leq \pi \quad \text{or} \quad 0 \leq \langle l'_1, l'_2 \rangle \leq \pi \leq \langle l'_1, l'_3 \rangle$$

The other configurations are equivalent since they are obtained by replacing all angles by their

opposites. In the first case, the half-line l'_1 and the half-line l'_2 are in half-planes separated by the line l'_3. In the second case, the half-line l'_2 and the half-line l'_3 are in half-planes separated by l'_1. The line l_2 separates the half-line l_1 and the half-line l_3. Thus, from the previous results, the half-line l'_1 and the half-line l'_3 are separated by the line l'_2 and the half-lines l'_1 and l'_2 (or l'_3 and l'_2) are therefore in the same half-plane with respect to l'_3 (or l'_1). We conclude that both the two cases are impossible, which proves that the relation (2) holds. In Figure 3, the separating lines have been indicated by prolonging the half-epipolar lines with dashed lines.

Because the orientation of each plane is arbitrary, it should be understood that the property we proved means that:

$$\text{If} \begin{cases} 0 \leq \widehat{\langle l_1, l_2 \rangle} \leq \widehat{\langle l_1, l_3 \rangle} \leq \pi \\ \text{or} \\ \pi \leq \widehat{\langle l_1, l_2 \rangle} \leq \widehat{\langle l_1, l_3 \rangle} \leq 2\pi \end{cases} \text{then} \begin{cases} 0 \leq \widehat{\langle l'_1, l'_2 \rangle} \leq \widehat{\langle l'_1, l'_3 \rangle} \leq \pi \\ \text{or} \\ \pi \leq \widehat{\langle l'_1, l'_2 \rangle} \leq \widehat{\langle l'_1, l'_3 \rangle} \leq 2\pi \end{cases}$$

A similar reasoning allows us to verify that if:

$$0 \leq \langle l_1, l_2 \rangle \leq \pi \leq \langle l_1, l_3 \rangle$$

then

$$0 \leq \langle l'_1, l'_2 \rangle \leq \pi \leq \langle l'_1, l'_3 \rangle$$

This is illustrated in the bottom row of diagrams in Figure 3.

By considering the pencils of epipolar planes and lines, it is possible to gain an intuitive interpretation of this result. Since all the epipolar planes contain the line $\langle C, C' \rangle$, an ordering can be defined by considering the angles between them, provided that an arbitrary orientation is chosen for these angles. This ordering induces two similar orderings, $\succ$ and $\succ'$, on the pencils of epipolar lines, which are compatible, modulo an arbitrary orientation, as illustrated by Figure 4. This means that if l_1, l_2, l_3 are epipolar half-lines of the first image and l'_1, l'_2, l'_3 are the corresponding epipolar half-lines in the second image, then

$$l_1 \succ l_2 \succ l_3 \Longrightarrow l'_1 \succ' l'_2 \succ' l'_3 \text{ or } l'_3 \succ' l'_2 \succ' l'_1.$$

The epipolar ordering is a strong constraint, which allows us to find out if a pair of points of

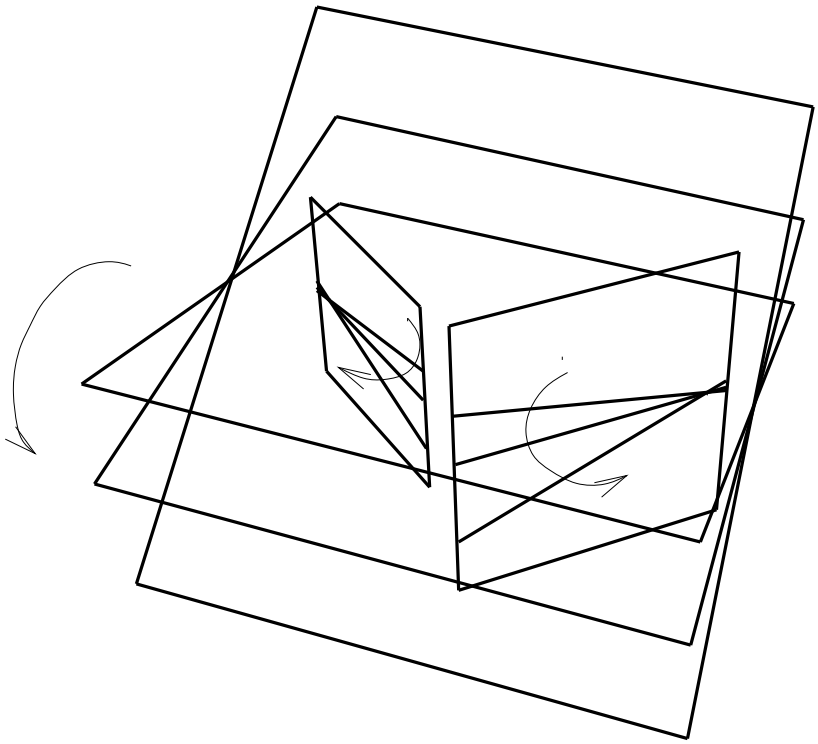

Figure 4: Ordering on the retinal planes induced by the ordering of the epipolar planes

$\mathcal{R} \times \mathcal{R}'$ is a pair of epipoles compatible with a set of correspondences, using the simple procedure described as Algorithm 1.

Algorithm 1: verification of epipolar ordering

- Chose an arbitrary pair of corresponding points (m_0, m'_0).
- For each correspondence, (m_i, m'_i), compute the angles $\alpha_i = \langle \mathbf{em}_0, \mathbf{em}_i \rangle$ and $\alpha'_i = \langle \mathbf{e}'\mathbf{m}'_0, \mathbf{e}'\mathbf{m}'_i \rangle$.
- Sort the α_i and α'_i by increasing values.
- Verify that the order of the α_i is either identical to or the opposite of the order of the α'_i.

Unlike the epipolar transformation, the epipolar ordering constraint is not a mere consequence of the projective camera model. It also involves the visibility constraint, which comes from the physical world. The observed points must lie in front of the focal planes of the cameras. This constraint has been known for some time (see for example [10]); however the formulation presented here is new in that it involves only comparisons in the image, and no 3-D reconstruction. Two other related pieces of work that formalize different aspects of this constraint are Cheirality invariants [6] and cones of visibility [22, 23]. The ordering constraint is very useful for our purposes, since we want first to try to estimate the epipoles separately in each image, and thus need a test for consistency of the pairs of epipoles.

3 The Sturm method

3.1 An outline

Sturm's method is based on a basic property of the epipolar transformation: as homography between pencils of epipolar lines, it leaves the cross-ratio invariant. That property enables us to compute separately the two epipoles from seven correspondences between two images. This number is expected to give a finite number of solutions, since the epipolar transformation is precisely defined by seven parameters. In Faugeras and Maybank [3] have traced the problem back to Chasles [1]. It has been solved by Hesse [8] and nicely summarized by Sturm [24]. The following algebraic

formulation of this method was presented by Maybank and Faugeras [18] where more details can be found.

Four points: *Four points yield a fourth degree polynomial constraint on the coordinates of the epipoles* $\mathbf{e}$, $\mathbf{e}'$ *of the two images.*

Let $\mathbf{q}_i \leftrightarrow \mathbf{q}'_i, 1 \leq i \leq 4$ be four point correspondences.

The equality of the cross-ratios of the lines $\langle \mathbf{e}, \mathbf{q}_i \rangle$, $1 \leq i \leq 4$ and of the lines $\langle \mathbf{e}'\mathbf{q}'_i \rangle$, $1 \leq i \leq 4$, can be written

$$\lambda_{1234} = \lambda'_{1234} \text{ where } \lambda_{1234} = \frac{(\mathbf{e} \times \mathbf{q}_4).\mathbf{q}_2}{(\mathbf{e} \times \mathbf{q}_4).\mathbf{q}_1} \frac{(\mathbf{e} \times \mathbf{q}_3).\mathbf{q}_1}{(\mathbf{e} \times \mathbf{q}_3).\mathbf{q}_2}, \lambda'_{1234} = \frac{(\mathbf{e}' \times \mathbf{q}'_4).\mathbf{q}'_2}{(\mathbf{e}' \times \mathbf{q}'_4).\mathbf{q}'_1} \frac{(\mathbf{e}' \times \mathbf{q}'_3).\mathbf{q}'_1}{(\mathbf{e}' \times \mathbf{q}'_3).\mathbf{q}'_2} \quad (3)$$

Six points: *Six correspondences* ($\mathbf{q}_i \leftrightarrow \mathbf{q}'_i, 1 \leq i \leq 6$) *constrain* $\mathbf{e}$ *to lie on a plane cubic.* Replacing $\mathbf{q}_4 \leftrightarrow \mathbf{q}'_4$ successively by $\mathbf{q}_5 \leftrightarrow \mathbf{q}'_5$ and $\mathbf{q}_6 \leftrightarrow \mathbf{q}'_6$, we obtain three equations of the form shown in Eq. (3).

By performing the change of projective coordinates

$$\begin{array}{lllll} \mathbf{q}_1 & = & (1,0,0)^\top & \mathbf{q}'_1 & = & (1,0,0)^\top \\ \mathbf{q}_2 & = & (0,1,0)^\top & \mathbf{q}'_2 & = & (0,1,0)^\top \\ \mathbf{q}_3 & = & (0,0,1)^\top & \mathbf{q}'_3 & = & (0,0,1)^\top \\ \mathbf{q}_4 & = & (1,1,1)^\top & \mathbf{q}'_4 & = & (1,1,1)^\top \end{array}$$

and introducing the quadratic transformation Φ_0, defined by $\Phi_0(\mathbf{x}) = (x_2x_3, x_3x_1, x_1x_2)^\top$, the three equations (3) are simplified:

$$\frac{u_1q_1 - u_3q_3}{u_2q_2 - u_3q_3} = \frac{u'_1q'_1 - u'_3q'_3}{u'_2q'_2 - u'_3q'_3}. \quad (4)$$

In equation (4), u_i are the coordinates in the first image of $\mathbf{u} = \Phi_0(\mathbf{e})$, and q_i are the coordinates of $\mathbf{q} = \mathbf{q}_4, \mathbf{q}_5, \mathbf{q}_6$. The primes designate corresponding quantities in the second image.

Equation (4) is linear in the coordinates of $\mathbf{u}'$, and can be written $\mathbf{a}_q(\mathbf{u}).\mathbf{u}' = 0$. There are three such equations, obtained with $\mathbf{q} = \mathbf{q}_4, \mathbf{q}_5, \mathbf{q}_6$. Since they have a common solution $\mathbf{u}'$, the following

coplanarity constraint must be satisfied:

$$f_u(\mathbf{u}) = (\mathbf{a}_4(\mathbf{u}) \times \mathbf{a}_5(\mathbf{u})).\mathbf{a}_6(\mathbf{u}) = 0 \tag{5}$$

After factoring out a common term and applying the quadratic transform Φ_0^{-1}, this is found to be a cubic polynomial constraint on $f(\mathbf{e}) = 0$.

Seven points: *If an additional correspondence* $\mathbf{q}_7 \leftrightarrow \mathbf{q}'_7$ *is available, then only three solutions for* $\mathbf{e}$ *are possible.*

Replacing $\mathbf{q}_6 \leftrightarrow \mathbf{q}'_6$ by $\mathbf{q}_7 \leftrightarrow \mathbf{q}'_7$, we find a second cubic constraint, $g(\mathbf{e}) = 0$. In the generic case, the cubics f and g meet at nine points, among them are the epipoles $\mathbf{e}$ compatible with the seven correspondences. Six of the intersection points are known: the points $\mathbf{q}_i, 1 \leq i \leq 5$, and the point $\mathbf{b}$, such that $\mathbf{a}_4(\Phi_0(\mathbf{b})) = \lambda \mathbf{a}_5(\Phi_0(\mathbf{b}))$. The three remaining intersections are the three epipoles compatible with the seven correspondences.

3.2 An example

We give an example to illustrate the Sturm method. The motion of the camera is the translation $(-7, 1, 7)^T$. Figure 5 shows the part of the retinal plane containing the 512×512 image, and a zoom into the image, showing the special points. The seven numbered points are the correspondences. It can be seen that the first 5 are common to the two cubics. The four other common points are the point $\mathbf{b} = (177.07, 238.16)^T$, and the three epipoles compatible with the 7 correspondences: $\mathbf{e}_1 = (-393.98, 390.46)^T$, $\mathbf{e}_2 = (313.46, 187.95)^T$, $\mathbf{e}_3 = (170.78, 229.78)^T$. By exchanging the role of the two images, the possible epipoles that are found are $\mathbf{e}'_1 = (-393.98, 390.46)^T$, $\mathbf{e}'_2 = (311.06, 189.86)^T$, and $\mathbf{e}'_3 = (169.04, 229.29)^T$. The pairing could also be verified by using the epipolar ordering constraint presented in Sec. 2.2 . Another way to check the pairing is to compute the epipolar homography from the epipoles and the point correspondences. This gives the fundamental matrices [14]. If the intrinsic parameters are known, then we can check whether the essential matrices satisfy the decomposability constraint [9, 16].

(a) Overall view

(b) Enlarged view

Figure 5: The Sturm method. The three possible epipoles are among the nine points of intersection of the two cubics. Five of these points are the correspondences used to define the cubics, and a sixth particular point can be eliminated.

3.3 Two typical displacements

The experimental part of this chapter is illustrated with two examples of typical displacements whose values are shown as Table 1. The first displacement yields epipoles within the image, whereas the second displacement yields epipoles that lie far outside. This difference leads to very different behaviors for the recovery algorithms. Since, stability results, in this case, are comparable for the image before and after displacement, we show only the results for the image before displacement.

Table 1: The two displacements used to illustrate the recovery algorithms. Note: The motion is specified in the first camera coordinate system (X and Y axis aligned with the image coordinate system). The first displacement is dominated by a translation perpendicular to the image plane, and the second displacement by a translation parallel to the image plane. To simulate a general motion, we have also added a rotational component. The axis of rotation is the direction of the rotation vector, and its angle is the norm of that vector.

	rotation			translation			correct value of epipole	
displacement 1	0	.05	0	0	0	400	214.062	255.648
displacement 2	0.1	0	0	50	20	20	2033.91	1409.83

The exact displacement fields used are shown in Figure 6. We start with 3D points scattered randomly in a cube centered 2 meters in front of the camera, and from a projection matrix $\mathbf{P}$ being obtained by calibrating a real camera with respect to the coordinate system associated to a grid placed 2 meters in front of the camera. The horizontal and vertical focal lengths in pixel units are respectively 625 and 934 (the aspect ratio was not 1) and the size of the image is 512×512 pixels. The 3D points are projected into the first image using $\mathbf{P}$. One of the two displacements is then applied to $\mathbf{P}$, resulting in another projection matrix $\mathbf{P}'$, which is used to project the 3D points into the second image. To obtain noisy correspondences, we add Gaussian noise of variance σ.

A hint on the relative stability of the method is provided by observing the evolution of the cubics as a function of image noise.

The first series is obtained with Displacement 1. In Figure 7 four cubics are superimposed at the noise levels of 0.1, 0.5, and 1 pixel. Although there are several intersections, making the figure difficult to read, it can be seen that the main intersection point remains approximatively near the

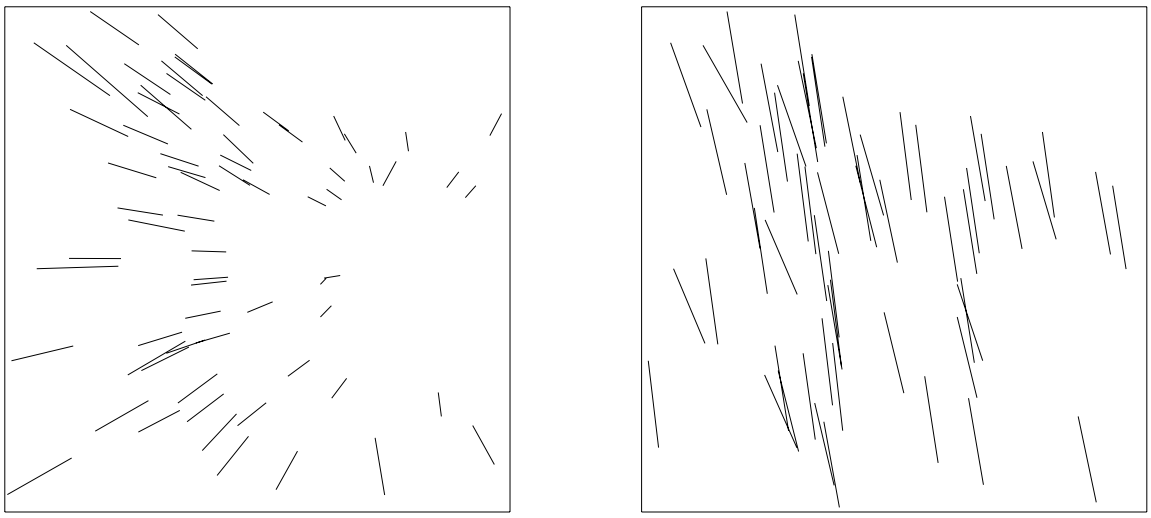

(a) First displacement

(b) Second displacement

Figure 6: Displacements fields. The line segments join each point in the image before displacement with its correspondent in the image after displacement.

image center.

The second series is obtained with Displacement 2. A global view of the retinal plane with five cubics is given in Figure 8 for the two noise levels of 0.1 and 1 pixel. A zoom to the vicinity of the epipole is also given for noise levels of 0.1, 0.5, and 1 pixel. Clearly, the intersection area is less well localized than in the previous case.

The noisy cubics lie farther apart from the exact epipole in the case where the epipole is far from the image. An intuitive explanation is as follows: the cubics used in Sturm's method are entirely determined by the nine points: $\mathbf{q}_i$, $1 \leq i \leq 6$, $\mathbf{b}_i$, $1 \leq i \leq 3$. Adding noise to the correspondences is equivalent to applying a perturbation to the points that control the cubics. The effect of the perturbation is more important for parts of the cubics that lie far from the control points. This would suggest that when the epipoles lie far from the image center, the Sturm method would give a worse localization on the image plane (in terms of Euclidean metrics) than if they lie within the image. Whether such a metric is actually relevant or not depends on the tasks the epipoles are to be used for. However, knowing the sensitivity in terms of metric coordinates, we can always derive a characterization based on another metric.

4 Using Sturm's method

In this section, we try to turn Sturm's method into an algorithm.

4.1 Selecting the epipole: the exhaustive method

Principle: Details on the implementation of the Sturm's method can be found in Luong [11]. There is a closed-form solution that involves solving a polynomial of degree three (with the Cardano's formulas).

The solution gives either one real possible epipole or three real possible epipoles, all compatible with the seven correspondences. In case only one epipole is obtained, its value can be directly used in a subsequent averaging scheme. However, in most of the cases, there will be three solutions. Therefore, selecting the correct epipole demands the use of more than seven correspondences. The Sturm method is first applied to each subset of seven correspondences, yielding a list of triplets of candidates. When there is only one epipole compatible with a subset, its value is simply duplicated three times, and the general scheme is run unchanged. False candidates are compatible only with the

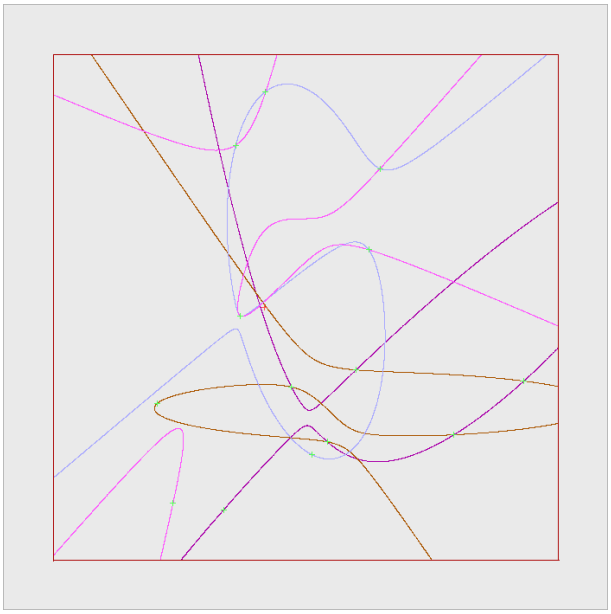

(a) Noise level 0.1 pixel

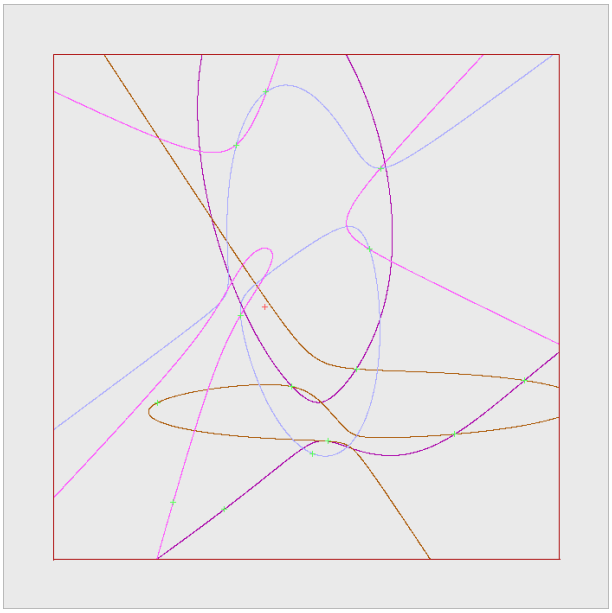

(b) Noise level 0.5 pixel

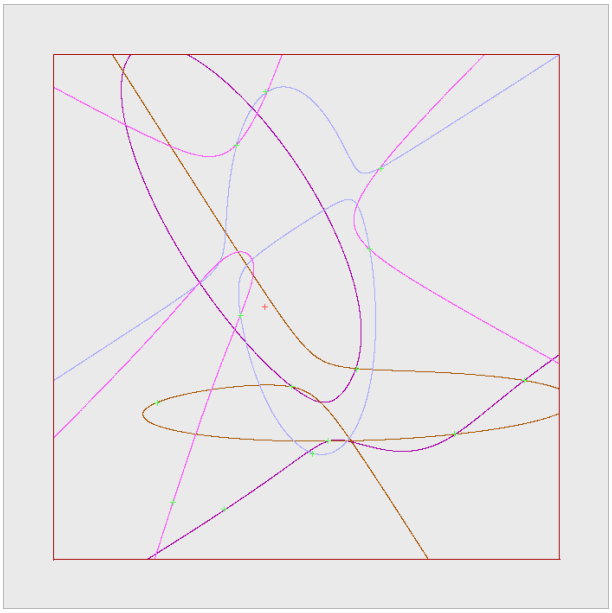

(c) Noise level 1 pixel

Figure 7: Displacement 1: four cubics The frame represents the image area. The main intersection point has a relatively stable location.

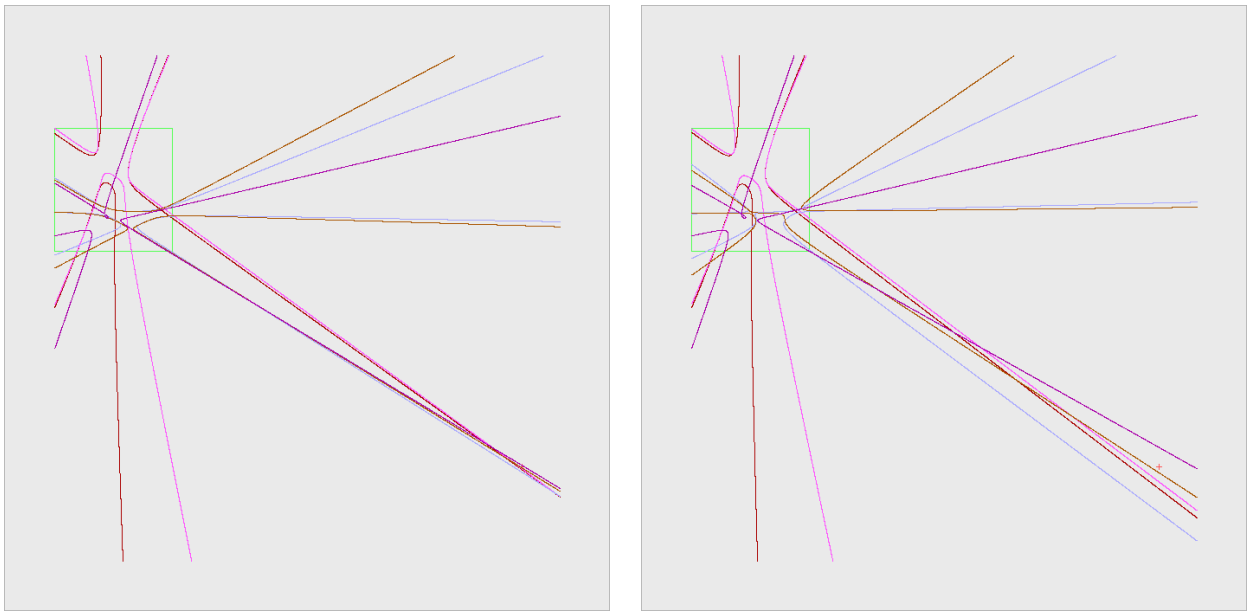

(a) Noise level 0.1 pixel

(b) Noise level 1 pixel

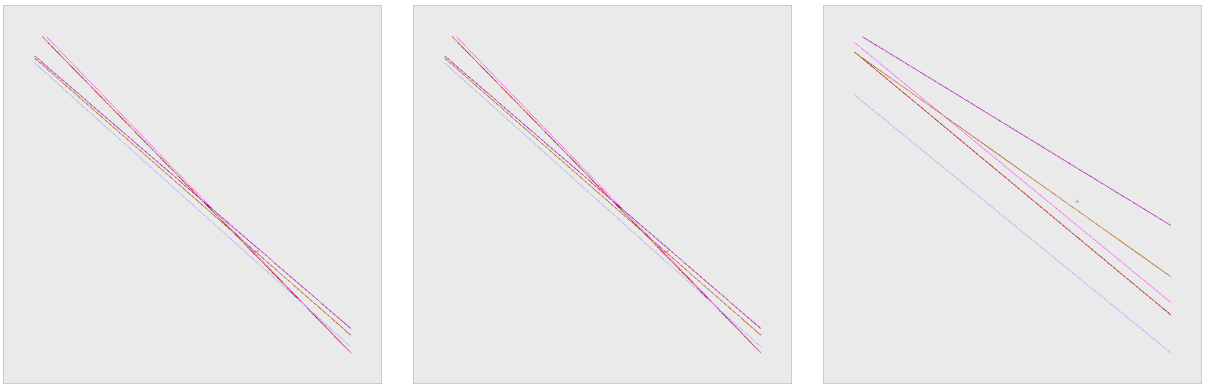

(c) Noise level 0.1 pixel, detail

(d) Noise level 0.5 pixel, detail

(e) Noise level 1 pixel, detail

Figure 8: Displacement 2: five cubics obtained with different noise levels. The frame represents the image area. Parts (c), (d), (e) show the vicinity of the epipole for three noise levels. The intersection area is not well localized.

subset of correspondences that enabled us to find them, whereas the good candidate is compatible with all the subsets of correspondences. As soon as eight points are available, an exhaustive selection procedure, described below, can be applied. It is very simple, but computationally expensive.

Algorithm 2: Sturm method with exhaustive selection

- Apply the Sturm method n times. This gives n triplets of points.
- Pick a point in each of the n triplets (total 3^n combinations).
- Compute a measure accounting for how spread apart the cluster of n selected points are (for example, the diameter of the smallest circle that contains all the n points).
- Keep the configuration giving the minimum diameter.
- Apply an averaging operator to the n points obtained.

We have tried several operators to evaluate the spread of the cluster, and also to perform the final averaging, but the differences were not significant.

Results and discussion: The behavior of the Sturm method with exhaustive selection is illustrated by Tables 2 and 3, in the minimal case $n = 8$. It is clear that the results can be very unstable, even with low noise, illustrating the difficulty that can be encountered when trying to turn an algebraic approach into an algorithm. One drawback of the method is that if the number of correspondences used is small, then the same points are often used several times, which leads to several false candidates lying in close proximity, and thus likely to be confused with the good epipole. Trying all the subsets of seven points with a large set of correspondences, however, would be too computationally expensive.

4.2 Robust statistics: using a random consensus procedure

Principle The goal is to improve the previous algorithm without changing the core procedure, the Sturm method from seven correspondences. In order to be able to consider more correspondences without a considerable increase of computation time, the exhaustive selection procedure is replaced by the random sampling consensus (RANSAC) introduced in the field of image under-

Table 2: Displacement 1: Results of the Sturm method with exhaustive selection.

noise	algorithm result	candidate epipoles triplets		
0.1 pixel		217.40 246.27	294.41 192.39	190.14 264.99
		219.73 274.79	279.38 350.68	329.88 405.74
		212.37 365.30		
	mean value	214.38 256.50	161.00 435.87	198.60 405.10
	214.39 272.31	209.33 274.80	88.19 363.39	212.94 254.61
	standard dev.	214.02 251.19		
	25.41	211.00 258.42	32.27 246.94	323.46 236.95
		216.89 250.72	164.53 290.62	271.92 200.29
0.5 pixel		168.55 251.34	212.95 226.10	297.03 174.50
		298.45 399.59		
		210.50 367.51		
	mean value	215.97 259.68	165.65 445.99	203.33 418.14
	209.83 290.65	204.56 272.20	90.72 358.99	208.91 250.75
	standard dev.	212.90 234.28		
	56.06	195.11 272.08	24.92 277.29	323.12 236.14
		172.59 268.51	275.04 197.31	223.67 237.51
1 pixel		201.00 208.02	145.58 233.57	307.37 152.37
		239.37 381.65		
		207.70 370.94		
	mean value	218.74 263.29	173.70 466.48	212.60 441.50
	202.57 281.99	199.35 269.86	93.98 353.31	204.71 246.64
	standard dev.	209.71 214.52		
	57.00	163.98 298.59	11.28 324.60	322.65 234.95
		180.72 249.05	279.15 194.81	227.63 228.00

Table 3: Displacement 2: Results of the Sturm method with exhaustive selection.

noise	algorithm result	candidates epipole triplets		
0.1 pixel		2364.24 1646.16	184.80 91.54	321.73 208.99
		790.92 684.22	277.31 342.92	364.16 403.48
		1917.58 1335.27	219.92 360.81	374.40 444.31
	mean value	1772.02 -396.31	8466.96 4576.25	9682.96 4972.67
	1821.20 1085.56	1857.21 1316.17	190.07 282.78	124.92 288.21
	standard dev.	2022.09 1390.05		
	603.46	1819.15 1269.88	243.77 154.26	324.50 239.16
		2026.35 1439.05	1039.95 1426.21	-68.44 545.90
0.2 pixel		322.29 211.65	184.10 93.68	2879.72 2013.39
		278.66 343.53	368.18 410.75	536.14 530.28
		219.98 360.69	1817.51 1270.81	366.24 438.93
	mean value	-2991.66 -1004.45	-3569.01 -1554.60	3573.79 -1365.63
	26.65 295.05	125.03 288.11	1717.15 1242.44	189.89 282.72
	standard dev.	2010.12 1370.60		
	873.44	324.71 239.66	245.36 155.07	1653.81 1162.14
		-75.91 550.58	1118.38 1505.55	2025.66 1474.49

standing by Fischler and Bolles [4]. In the usual methods, the largest data set is used to obtain an initial solution by computing the unknown parameters with an averaging operator. By contrast, the RANSAC method use initial data sets S of size large enough to allow for the computation of the parameters M, and then enlarges these sets by incorporating data coherent with the parameters computed from the initial data set (a compatibility threshold t_1 must be set). A number of N_1 initial sets are obtained by random sampling. The parameters computed from such a set are accepted if the consensus set S^* has a cardinality above threshold t_2. One important advantage of RANSAC over the methods based on an averaging scheme is that it is a robust method, in the sense that it is not affected by outliers which might be caused by false matches.

In the problem that we are considering, a data point is a subset of seven points, and the model is a 2D point (the epipole) and an error radius. Depending on the position of the epipole, the deviation on the curve induced by noise is more or less large. The minimum number of data points is two distinct subsets of seven points. The adaptation of the RANSAC algorithm to our problem is presented as Algorithm 3. There are some differences from the original algorithm, which are detailed in Luong [11].

Algorithm 3: Sturm method with random consensus

Repeat until a satisfying epipole is found (N_1 tries, then exit with failure):

- *Initialize the model [Point-diameter].* Repeat until a satisfying model is found (N_2 tries, then exit with failure):
  - Take two random disjoint subsets of seven correspondences, S_1 and S_1'.
  - Compute the triplets of epipoles $E = (\mathbf{e}_1, \mathbf{e}_2, \mathbf{e}_3)$ and $E' = (\mathbf{e}_1', \mathbf{e}_2', \mathbf{e}_3')$ from S_1 and S_1'.
  - Select the pair of epipoles $(\mathbf{e}_i, \mathbf{e}_i') \in E \times E'$ which gives the smallest distance $d_1(\mathbf{e}_i, \mathbf{e}_i')$.
  - If $d_1 < t_0$, take $\mathbf{e} = (\mathbf{e}_i + \mathbf{e}_i')/2$, and $r = d_2(\mathbf{e}_i, \mathbf{e})$, else try again.
- *Find a consensus set for* $(\mathbf{e}, r)$. Repeat to obtain a significant number N_3 of samples of seven correspondences:
  - Pick up a random subset of seven correspondences S'.
  - Compute the triplet of epipoles $E = (\mathbf{e}_1, \mathbf{e}_2, \mathbf{e}_3)$ from S'.
  - If one of the $\mathbf{e}_i$ is in the disc of center $\mathbf{e}$ and radius $r \times t_1$, increment the number of consensus points N^* and update the model: $\mathbf{e} = \frac{N^*\mathbf{e}+\mathbf{e}_i}{N^*+1}$, $r = \sup(r, d_2(\mathbf{e}, \mathbf{e}_i))$.
- If $\frac{N_3 - N^*}{N_3} > t_2$ (the consensus set represents a large enough fraction of the number of samples) give $\mathbf{e}$ as final result, otherwise try again, and eventually exit with failure giving the epipole that had the largest consensus set.

Results and discussion Some results are shown in Tables 4 and 5. Experiments were carried out with 58 correspondences, and the "standard" parameters $N_1 = 100$, $N_2 = 2 \times 58$, $N_3 = 2 \times 58$, $t_0 = 0.05$, $t_1 = 1.2$, $t_2 = 0.5$. The approach is satisfying in the case where the epipole is within the image or close to it, but remains too sensitive to noise if the epipole is far from the image.

During the model initialization stage, if two good epipoles (the one from S_1 and the one from S_1') are separated (because of the perturbation induced by noise) by a distance comparable to the size of the image, then it is very likely that instead of these epipoles, the points selected by the procedure to instantiate the model will be two false epipoles which both lie inside the image, since the distance between these two points could be less than the distance between the two epipoles

which are perturbed differently.

It thus appears that the basic source of trouble is the unstable results produced by the Sturm method, which is the core of the algorithm. The Sturm method does not take explicit account of noise, and uses algebraic operations that are quite sensitive.

Table 4: Displacement 1: Results of the Sturm method with random consensus

noise	epipole found		error radius	% consensus	nb of tries
0	214.06	255.64	0.000021	0.676	1
0.1	214.40	254.72	10.09	0.882	3
0.2	214.45	255.19	7.65	0.544	2
0.5	215.60	252.42	16.12	0.603	43
1	217.54	258.32	26.00	0.507	81
2	215.23	236.34	11.87	0.199	100/fail

Table 5: Displacement 2: Results of the Sturm method with random consensus

noise	epipole found		error radius	% consensus	nb tries
0	2033.80	1409.83	0.07	0.966	1
0.1	1797.28	1264.76	370.93	0.569	22
0.2	1666.87	1179.85	535.60	0.397	100/fail
0.5	160.90	459.66	11.72	0.086	100/fail
1	166.13	415.36	12.34	0.138	100/fail

5 The cubics method

In this section, we investigate approaches that take explicit account of noise and data redundancy. We have seen that the Sturm method determines two cubics which both contain the epipole. A natural approach, which copes well with a data set consisting of a large number of correspondences, is to compute several of these cubics and then to try to find a common point for all of them. As this point cannot be localized exactly in the presence of noise, we must use an approximate intersection using a least-squares technique.

5.1 Minimizing an algebraic criterion

Principle From the $2n$ cubics $f_i(\mathbf{x})$ and $g_i(\mathbf{x})$, computed in a common coordinate system, it is possible to obtain with an arbitrary precision the point $\mathbf{x}$ that minimizes the sum:

$$S(\mathbf{x}) = \sum_{i=1}^{n} \left(f_i(\mathbf{x})^2 + g_i(\mathbf{x})^2 \right) \tag{6}$$

In this expression, $f_i(\mathbf{x})$ et $g_i(\mathbf{x})$ designates the cubics written in the original retinal coordinate system of the camera.

The polynomial S is homogeneous and of degree six. By setting one of the variables to 1, we obtain a polynomial of degree six with two variables, $S(x, y)$. Its minimum can be computed with arbitrary precision as follows. Let $S_x(x, y)$ and $S_y(x, y)$ be the partial derivatives of S with respect to x and y, which must be zero for any extremum of S. The resultant $R(y)$ of $S_x(x, y)$ and $S_y(x, y)$ with respect to x, is a polynomial of degree 25 with one variable. It is thus possible to obtain all its zeros y_i with arbitrary precision. For each of the 25 zeros, we then solve the two polynomials of degree 5: $S_x(x, y_i) = 0$ and $S_y(x, y_i) = 0$. This gives x_i as the common zero of the two polynomials. Once this is done, the global minimum is obtained by comparing the 25 values of $S(x_i, y_i)$. Other local minima can also be retained.

Results and discussion The approach has been implemented using the symbolic algebra system MAPLE, which allowed us to use high precision floating operations (30 to 40 digits). Some results, obtained using 10 cubics, are presented in Table (6).

As already shown, the typical behavior of this method depends on the proximity of the epipole to the image center. Where the epipole is quite distant, it is found among the local minima of $S(x, y)$ at low noise levels, whereas the global minimum is a false point inside the image. Thus the method does not work.

In the case where the epipole is within the image, the precision of localization is satisfying, and it is actually found as the global minimum. One explanation for this behavior of the algorithm is that the criterion (6) does not represent the quantity to be minimized, which is the sum of the squared distances of the point $\mathbf{x}$ to the cubics $f_i(\mathbf{x})$ and $g_i(\mathbf{x})$. Thus the criterion (6) favors the points in the image, whose residual values are lower for the same distances. This observation parallels the more quantitative observation of [12] for the estimation of epipoles though the fundamental matrix

using the linear algebraic expression of the epipolar constraint.

Table 6: Displacement 1 and 2: results of the algebraic intersection method. Note: For each noise level the first few local minima of the sum of the squares of cubics are shown. The minimum corresponding to the true epipole is in boldface. It is always selected for the Displacement 1, but is not selected for the Displacement 2 in the presence of noise.

(a) Displacement 1

noise	minima found		residual
0	**214.06**	**255.64**	10^{-13}
	174.92	323.41	.00027
	188.90	293.18	.00033
0.1	**215.58**	**254.54**	.000041
	176.93	316.59	.00029
	186.13	295.20	.00031
0.2	**211.63**	**256.32**	.00018
0.5	**184.22**	**280.70**	.00030
1	**178.20**	**278.28**	.00049
	300.12	240.88	.02949
	265.16	213.82	.03170
	253.73	215.18	.03182
	278.54	218.25	.03191
2	**175.63**	**314.82**	.00596
	149.35	376.04	.00703
	165.20	361.87	.03853
	228.23	117.79	.2526
	194.48	113.32	.2927
	10.68	25.23	.5132
	68.18	58.68	.6871

(b) Displacement 2

noise	minima found		residual
0	**2033.79**	**1409.82**	10^{-6}
	163.74	343.79	.00021
	206.55	206.59	.00984
	196.97	237.34	.01200
	300.34	256.43	.02244
	267.39	214.68	.04562
	1404.3	974.87	20.21
0.1	163.66	343.91	.00022
	207.09	206.65	.00980
	197.02	237.64	.01208
	299.07	255.97	.02165
	265.84	217.85	.03695
	2008.0	**1398.8**	17.70
	1528.4	1065.9	26.73
0.2	163.59	344.02	.00023
	207.68	206.75	.00975
	197.07	237.94	.01216
	297.53	255.31	.02083
	265.07	220.81	.03075

5.2 A graphical approach

Principle The graphical approach enables us to find approximate intersections of n polynomial curves in the plane, while avoiding the bias previously described. The basic algorithm shown as Algorithm 4 bellow is a simple implementation. Its principle is similar to that of Hough transforms. It relies on the fact that for a plane polynomial curve, if one of the two variables is fixed, the possible values of the other variable are easily obtained by solving a polynomial in one unknown. If we use

a sampling of the X-axis that is sufficiently fine with respect to the size of the cells, at least one cell in a column will be marked for each branch, for all but the parts of the curve with steep slope. The other cases are adequately dealt with using a similar fine sampling on the Y-axis.

Algorithm 4: approximative intersection

- Divide the search area $[x_{min}, x_{max}] \times [y_{min}, y_{max}]$ in rectangular cells $dim_x \times dim_y$.
- For each subset i of seven correspondences, compute the two cubics $c_{2i} = f$ and $c_{2i+1} = g$.
- For each cubic c_i
  - For x from x_{min} to x_{max}
    - Solve numerically the equation $c_i(x, y) = 0$ with $y_{min} \leq y \leq y_{max}$.
    - Mark all the cells containing at least one point satisfying the previous equation with index i.
  - For y varying from y_{min} to y_{max}
    - Solve the equation $c_i(x, y) = 0$ with $x_{min} \leq x \leq x_{max}$.
    - Mark all the cells containing at least a point satisfying the previous equation with index i.
- Sort the cells by the number of cubics that were met.
- Keep the N first cells.

The parameters associated with this algorithm are the size of the search area $[x_{min}, x_{max}] \times [y_{min}, y_{max}]$, the size of the cells $dim_x \times dim_y$ and the number N of cells to be kept.

The optimal choice of the size of cells depends on the expected noise. If the noise is small, it is possible to use small cells (the width is a few pixels) and to keep only the one that meets all the cubics. However, in the presence of much noise, for small cell sizes the right cell will not meet more cubics than the other cells, and thus will not be selected by the algorithm.

On the other hand, large cells tend to generate false intersections. For instance, if the size of the cell is close to the size of the image, since all the cubics by construction intersect the image, the algorithm will always detect spurious intersection cells in the image.

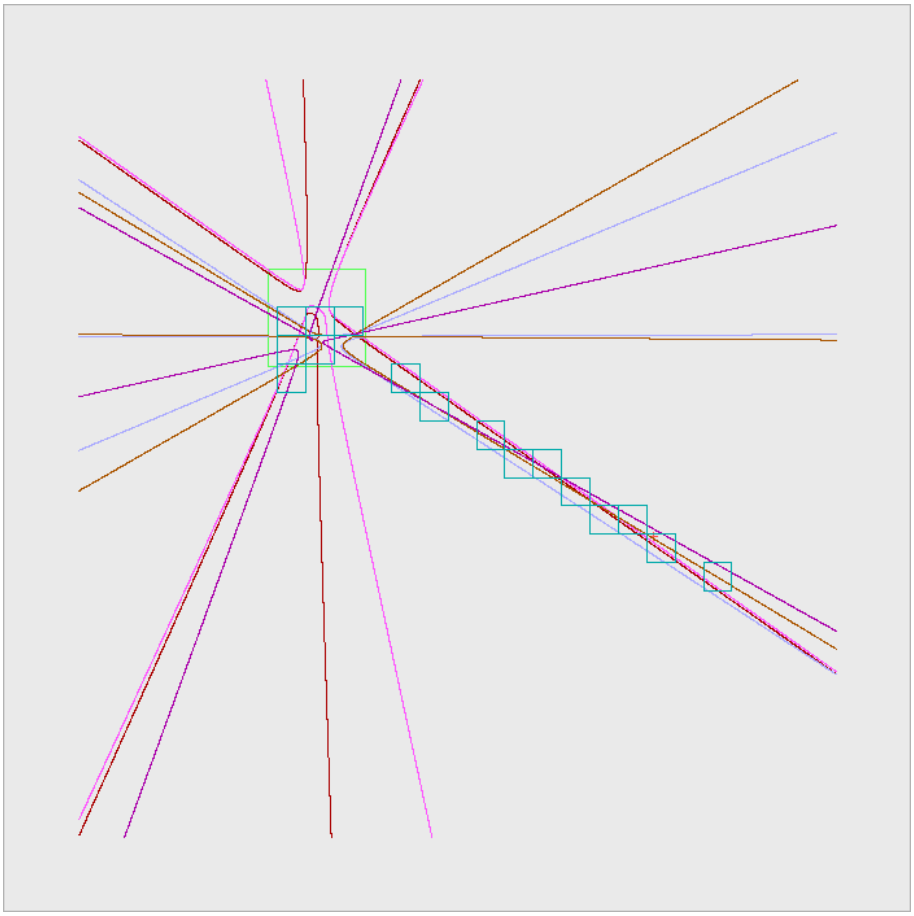

Figure 9: An example of cells found by the (graphical) cubics method

Results and discussion Figure 9 shows the 14 first cells of size 150×150 pixels found for Displacement 2, with 0.5 pixel noise.

With epipoles lying inside the image, the method was found to work. With distant epipoles, it is not possible above a certain noise level, to localize the cell containing the exact epipole, whatever the size of the cell, since that cell is no longer ranked first. The cells situated within the image would be given a better rank, exactly as in the algebraic method.

This suggests that there is an intrinsic bias with the cubics method, beyond the one we identified with the algebraic method.

The quantities in the Sturm method that are significant image measurements are the cross-ratio of epipolar lines. In transforming the equalities (3), the two members are multiplied by denominators. As long as exact quantities are concerned, there is no problem. But when considering approxi-

mations, when we are performing the minimization on the final equations, this amounts to weighting the equations which are eventually obtained by a certain quantity that depends on point coordinates. It is known that minimizing $\sum (\frac{a_i}{b_i} - \frac{a'_i}{b'_i})^2$ is not equivalent to minimizing $\sum (a_i b'_i - a'_i b_i)^2$, because in the second case, there is an unwanted weighting by $b_i b'_i$. In the section 6, we thus work only from the cross-ratio, and stop using the cubics. Before that, we explain how the cubics method could be used.

5.3 Using the cubics method to find candidates

The computational methods used to determine the fundamental matrix, which will be studied later, are based on non-linear minimization. To use such methods successfully we must choose of good starting point. There are almost always several local minima, but we are interested in finding the global minimum. If we don't have estimates that are sufficiently good, a way to proceed is to make a division of the search space, and then to start the minimizations by initializing using each of the points obtained in this way. This approach is not tractable if the size of the search space is large. An alternative way to proceed is then to try and select a certain number of possible candidates, using a heuristic approach. We now propose, as Algorithm 5, such an approach, based on the Sturm cubics, the epipolar ordering constraint, and the epipolar homography.

Algorithm 5: Construction of a list of pairs of epipoles

- Apply the cubics method in Image 1 and keep the N_1 first cells in $\mathcal{E}_1$.
- Apply the cubics method in Image 2 and keep the N_1 first cells in $\mathcal{E}_2$.
- For each element of $\mathcal{E}_1 \times \mathcal{E}_2$,
  - Verify if the epipolar ordering constraint is satisfied, and reject the element if it is not (experimentally this has helped remove some bad solutions).
  - Compute the epipolar homography using the least-squares method over the correspondences, and the residual ϵ_{ij}.
- Sort the elements of $\mathcal{E}_1 \times \mathcal{E}_2$ according to the values ϵ_{ij}, and keep the N_2 first ones.

The advantage of this method is that the search space for the individual epipoles is only two (the computation of the epipole in each image is decoupled from the computation of the epipole in the other image, when using the cubics method), and then strong constraints can be used to restrict the final list.

6 The cross-ratio method

The approach that we propose in this section is to use directly the cross-ratio of epipolar lines, and minimize their differences using non linear methods. We describe a few refinements to the basic idea. The results are compared with another method based on non linear minimization, the classical Fundamental matrix approach.

6.1 Principle

The principle is to start from a set of correspondences $\mathbf{q}_i \leftrightarrow \mathbf{q}'_i$, $1 \leq i \leq n$, and to consider subsets of four correspondences $j = \{j_1, j_2, j_3, j_4\}$, j_1, j_2, j_3, j_4 being indices of $\{1, \ldots, n\}$, all different. By writing the equality of the cross-ratios $\lambda_{j_1 j_2 j_3 j_4}$ and $\lambda'_{j_1 j_2 j_3 j_4}$ as defined in equation (3), we obtain an equation that constrains the position of the epipoles $\mathbf{e}$ and $\mathbf{e}'$.

We have four unknowns, the coordinates of the two epipoles, so that four subsets of correspondences are needed. With the Sturm method, if we allow ourselves to reuse the same points in several cross-ratios, then multiple solutions appear, which are difficult to discriminate between. If a large number of correspondences are available, then it is better to use disjoint subsets of correspondences. We search for the epipoles $\mathbf{e}$ and $\mathbf{e}'$ by minimizing the non linear criterion:

$$C(\mathbf{e}, \mathbf{e}') = \sum_j (\lambda_j - \lambda'_j)^2. \tag{7}$$

6.2 Taking uncertainty into account

All the configurations of four points do not yield cross-ratios with the same stability. For example, if two points among the four are identical, than the cross-ratio is singular. Thus its variance can be expected to be high when the distance between two points can be compared to the standard deviation on the positions of these points.

If we pose the classical hypothesis that the points are uncorrelated and their variance is uniform

and isotropic, then the variance of the cross-ratio is proportional to the variance of the measured points (an approximation correct to first order):

$$\sigma_{\lambda_j}^2 = \sigma^2 \|\nabla \lambda_j\|^2$$

where $\nabla \lambda_j$ designates the gradient of λ_j with respect to the eight-dimensional vector $(\mathbf{q}_{j_1}, \ldots, \mathbf{q}_{j_4})^T$, obtained by concatenation of the coordinates of the points $\mathbf{q}_{j_k}$.

To deal with uncertainty, the idea is to weight each term of the criterion (7) by the variance of $\lambda_j - \lambda'_j$ so that the contribution of the individual cross-ratios to the criterion will be inversely proportional to their variance. This reduces the influence of the unstable configurations. Since λ_j and λ'_j are independent, the variance of $\lambda_j - \lambda'_j$ is $\sigma_{\lambda_j}^2 + \sigma_{\lambda'_j}^2$, which leads to the new criterion:

$$C_1(\mathbf{e}, \mathbf{e}') = \sum_j \frac{(\lambda_j - \lambda'_j)^2}{\sigma_{\lambda_j}^2 + \sigma_{\lambda'_j}^2}. \tag{8}$$

6.3 Taking ordering into account

The cross-ratio depends on the order in which the points are labeled. It is known that the 24 labeling possibilities yield six distinct values. One of the problems encountered when using the cross-ratio method is that the labeling determined by choosing the subsets of four points is arbitrary. This implies that we will, for each subset, chose one of the six values without reason. The six representatives and the relations between them are:

$$\begin{aligned}
\{x_1, x_2, x_3, x_4\} &= \lambda \\
\{x_1, x_3, x_2, x_4\} &= 1 - \lambda \\
\{x_2, x_1, x_3, x_4\} &= \frac{1}{\lambda} \\
\{x_2, x_3, x_1, x_4\} &= 1 - \frac{1}{\lambda} \\
\{x_3, x_1, x_2, x_4\} &= \frac{1}{1-\lambda} \\
\{x_3, x_2, x_1, x_4\} &= 1 - \frac{1}{1-\lambda}.
\end{aligned}$$

They are obtained as the action of the permutation group on four symbols. The invariants of this action are the symmetries, and thus

$$\{x_1, x_2, x_3, x_4\} = \{x_2, x_1, x_4, x_3\} = \{x_3, x_4, x_1, x_2\} = \{x_4, x_3, x_2, x_1\}.$$

A first approach is to use for each subset of four points the sextet whose components are the six representatives just mentioned, and to measure the difference between the cross-ratios using a norm in $\mathbf{IR}^6$ space. In this approach, we need only the three representatives λ, $\frac{1}{\lambda}$ and $\frac{1}{1-\lambda}$, since only the differences are significant. We first tried this approach, using the L^2 norm which preserves derivability. It yields complicated formulas if uncertainty is also taken into account.

A second closely related approach is to perform the minimization on the functions $f(\lambda) - f(\lambda')$, where λ and λ' are the cross-ratios and f is the algebraic function associated with the cross-ratio, whose characteristic property is to have identical values for each orbit:

$$f(\lambda) = \frac{(\lambda^2 - \lambda + 1)^3}{\lambda^2 (1-\lambda)^2}. \tag{9}$$

The results obtained with these two approaches were comparable and unsatisfying. There are convergence problems, perhaps because of the complexity of the resulting criterion.

Let us now look closely at the values taken by the cross-ratios. We can define a partition of $\mathbf{IR}$ by taking the intervals delimited by the successive values $-\infty$, -1, 0, $\frac{1}{2}$, 1, 2, $+\infty$. Among these values are values corresponding to a configuration for which two of the four points are the same: $-\infty$, 0, 1, $+\infty$. This partition has the following property: given four points, and the six values of the cross-ratio obtained by a permutation of these points, each of the six intervals previously defined contains one, and only one of these six values. The Table 7 shows the action of the permutation on the values of the cross-ratio.

We conclude that, given four points, and one of these six intervals, it is always possible to bring the value of the cross-ratio into this interval just by applying a simple permutation on the order of the points. The permutation can be chosen very simply by considering only the interval that includes the initial cross-ratio, and the target interval. For instance, if the target interval is [0, 1/2], and the initial value of the cross-ratio λ is in [1 2], we have to apply the permutation $(1234) \rightarrow (2314)$, which is equivalent to taking the representant $1 - \frac{1}{\lambda}$. This third

Table 7: Permutations and values of the cross-ratio. If the initial value of the cross-ratio is in the interval listed in the first column, applying the permutations on the order of points listed in the subsequent columns will map the cross-ratio to a new interval.

1234	1324	2134	2314	3124	3214
λ	$1-\lambda$	$\frac{1}{\lambda}$	$1-\frac{1}{\lambda}$	$\frac{1}{1-\lambda}$	$1-\frac{1}{1-\lambda}$
$-\infty$ -1	2 $+\infty$	-1 0	1 2	0 $\frac{1}{2}$	$\frac{1}{2}$ 1
-1 0	1 2	$-\infty$ -1	2 $+\infty$	$\frac{1}{2}$ 1	0 $\frac{1}{2}$
0 $\frac{1}{2}$	$\frac{1}{2}$1	2 $+\infty$	$-\infty$ -1	1 2	-1 0
$\frac{1}{2}$1	0 $\frac{1}{2}$	1 2	-1 0	2 $+\infty$	$-\infty$ -1
1 2	-1 0	$\frac{1}{2}$1	0 $\frac{1}{2}$	$-\infty$ -1	2 $+\infty$
2 $+\infty$	$-\infty$ -1	0 $\frac{1}{2}$	$\frac{1}{2}$1	-1 0	1 2

approach has been incorporated into the minimization based algorithm. The advantage is that it requires only a mere comparison, and then a permutation of indices. Thus we can still use the formulas (8). In practice, by taking the ordering into account, we bring all the cross-ratios in a unique interval to obtain quantities which are comparable, and therefore avoid discrepancies in order of magnitude, which would result in favoring some quantities during minimization. Moreover, if we chose the representative of the cross-ratio between 0 and 1/2, then we can reduce the influence of the configurations of points which yield singular cross-ratios. These configurations are those where the line joining two points contains the epipole: the two associated epipolar lines are then identical and generally yield the forbidden values 0,1,-1,∞. Our choice reduces their influence because they would yield only the value 0, which doesn't influence the minimization process. In the case where ordering is not taken into account, or when non-bounded intervals are chosen for ordering, cross-ratios can assume arbitrarily large values for singular configurations. Intuitively, the points which are chosen in the image induce a division of the plane by their lines of mutual intersection. Each zone is separated from its neighbors by an asymptotic value of the criterion, which prevents effective minimization over the whole plane.

6.4 Experimental results

Results and discussion The minima obtained for the two reference displacements are presented in Tables 8 and 9. The precision is much better than with the Sturm method or the cubics method. Using the covariance and the permutations improves the results.

Table 8: Displacement 1: position of the exact minimum with the cross-ratio method. C: normalization by the covariance, P: applying the permutations.

noise	cross-ratios		cross-ratio + C		cross-ratio + P		cross-ratio + C + P	
0	214.062	255.648	214.062	255.648	214.062	255.648	214.062	255.648
0.1	213.758	258.841	213.097	255.321	212.231	258.55	213.592	255.647
0.2	215.425	262.478	212.57	255.342	209.852	261.277	212.895	255.368
0.5	217.774	265.963	211.362	256.181	203.865	272.656	210.455	255.471
1	220.193	266.939	208.379	262.064	206.664	274.999	208.471	257.147
2	222.84	267.821	195.454	279.067	212.881	254.316	212.328	256.518

Table 9: Displacement 2: position of the exact minimum with the cross-ratio method. C: normalization by the covariance, P: applying the permutations.

noise	cross-ratio		cross-ratio + C		cross-ratio + P		cross-ratio + C + P	
0	2033.81	1409.83	2033.8	1409.83	2033.8	1409.83	2033.8	1409.83
0.1	1246.02	960.101	2056.56	1425.43	1423.12	1043.82	2054.92	1424.38
0.2	1767.23	1108.08	2096.17	1450.8	1125.79	860.566	2085.77	1444.16
0.5	2028.21	1493.26	2134.76	1481.26	1001.31	792.913	2114.72	1465.22
1	2093.84	1381.41	2069.09	1446.9	1750.9	1100.31	2053.83	1427.84
2	1388.14	1108.41	2122.09	1484.4	1126.3	789.248	1605.51	1139.08

We can interpret the cross-ratios as angles between lines, making it clear that when the epipoles are far from the image, the computation yields less precise results. The angular differences are then less affected by a given displacement of the epipole than they would be if the epipole were closer to the image. When epipoles are distant, the sensitivity is higher in the direction orthogonal to the line joining the epipole to the image center so that the direction of the epipole can be recovered more accurately than its distance to the image center. Thus we again find the conclusions obtained from the analysis of the methods tried earlier. Here, however, less bias is induced by algebraic manipulations.

Statistical comparison To make an accurate statistical assessment of the performance of any method, we must change not only the image noise, as is often done, but also the displacements, as different displacements give rise to configurations whose stability properties are very different.

We use data points and a projection matrix $\mathbf{P}$ similar to those described in Sec. 3.3, Each trial consists of three steps:

- Take a random rigid displacement $\mathbf{D}$,
- Compute the exact fundamental matrix $\mathbf{F}_0$ from $\mathbf{D}$ and $\mathbf{P}$,
- Compute the projection matrix $\mathbf{P}'$ from $\mathbf{D}$ and $\mathbf{P}$,
- Project the 3D points in the two 512×512 retinas using $\mathbf{P}$ and $\mathbf{P}'$,
- Add Gaussian noise to the image points,
- Solve for the epipoles $\mathbf{e}$ and $\mathbf{e}'$
- Compute the relative distance of these epipoles with and those from $\mathbf{F}_0$.

We measure the error by the relative distance for each coordinate of the epipole:

$$\min\{\frac{|x - x_0|}{\min(|x|, |x_0|)}, 1\}$$

The results are compared with those of another method based on non-linear minimization, the classical Fundamental matrix approach [20, 2, 12, 5], because one of the goals of the paper was to investigate how direct methods to determine the epipoles compare with indirect methods that first compute the Fundamental matrix.

The Table 10 summarizes 100 trials. It shows the mean value of the relative distances obtained with the different versions of the cross-ratio method. Since the method is based on non-linear minimization, the choice of starting point is very important. We have illustrated the behavior of the method with two different choices. The first one is the exact epipole, the second is the linear indirect method to determine the fundamental matrix. The first initialization enables us to test the stability of the minimum, the second one (which is not too accurate [12].) lets us test the convergence properties of the algorithm.

The results confirm that taking into account the uncertainty and the permutations improve the results. When the initialization is appropriate, we obtain a minimum whose precision can be

Table 10: Statistic: Average relative distances obtained with the cross-ratio method. C: normalization by the covariance, P: applying the permutations. The initialization points tried are the exact value and the value obtained from the Fundamental matrix method.

method	noise 0.2 pixel		noise 1.0 pixel	
	exact	linear F-mat	exact	linear F-mat
cross-ratio	0.2108	0.2969	0.3446	0.5987
cross-ratio + C	0.1404	0.2200	0.2744	0.5496
cross-ratio + P	0.1429	0.2305	0.2651	0.5718
cross-ratio + P + C	0.1169	0.2158	0.2344	0.5395
fundamental matrix	0.1006	0.1222	0.2581	0.3437

compared to those obtained with the enhanced methods for the computation of the fundamental matrix [12].

The main shortcoming of the cross-ratio method is that it is quite sensitive to the choice of the initialization point. In practice, better results are obtained with the Fundamental matrix method.

7 Conclusion

We have studied the problem of directly computing the position of the epipoles in a pair of uncalibrated images based on the invariance of the cross-ratio. The method is based on an algebraic constraint, that allows a closed-form solution. However, we have shown that this approach is highly unstable, and have considered two iterative methods instead. We presented experimental results showing that the iterative methods improve the robustness of the method, which was initially unacceptable, and become usable in the final version with some precautions. The improvement is great. With one pixel of noise, for the first displacement tested, the relative error goes from 10% to 2%. For the second displacement, the first methods totally fail with as little as 0.1 pixel of noise, whereas the last method gives a relative error of only 2%. Thus, interestingly enough, there seems to be a trade-off between robustness and computational simplicity and mathematical elegance, as summarized in Table 11. The methods listed appear to have an increasing robustness to noise.

One of the goals of the paper was to investigate whether the direct methods based on the cross-ratio are a good alternative to methods based on the Fundamental matrix. The answer

Table 11: Summary of methods tried

manipulated quantity	obtained with	operations	complexity	unknowns
triplets of epipoles	7 points	clustering	closed form algebraic	2
plane cubics	6 points	approximative intersection	deterministic iterative	2
cross-ratios	4 points	non-linear minimization	non-deterministic iterative	4

seems to be generally no: used alone, the Fundamental matrix method generally gives a better precision. We have delimited the applicability of the direct methods. In particular, we have given several explanations of the fact that an epipole within the image is estimated more robustly than an epipole that lies far outside, a fact also found in [13] by other means. Although the direct methods eventually turn out to be less robust to noise than the methods based on the fundamental matrix, the direct methods might be useful in some situations. For example, the Sturm method is a good choice when trying to segment rigid objects moving independently in a scene from a pair of uncalibrated images, a representation that is compact and easy to compute, but only qualitatively useful for clustering [25].

Our investigation can also be seen as a case study in algebraic methods for geometric problems. We believe that the ideas developped in this paper, allowing us to turn an algebraic idea into a robust computational scheme could also be applied to other problems. For example, computing the invariants of six points from three images also involves intersecting cubics [21], and thus most of the methods we have investigated could be used to improve the robustness of the solution.

Acknowledgment

We thank Steve Maybank for fruitful discussions during the progress of this work, and the reviewers for their helpful remarks.

References

[1] M. Chasles. Question No. 296. *Nouv. Ann. Math.*, 14:50, 1855.

[2] O.D. Faugeras, Q.-T. Luong, and S.J. Maybank. Camera self-calibration: theory and experiments. In *Proc. European Conference on Computer Vision*, pages 321–334, Santa-Margerita, Italy, 1992.

[3] O.D. Faugeras and S.J. Maybank. Motion from point matches: multiplicity of solutions. *The International Journal of Computer Vision*, 4(3):225–246, 1990. also INRIA Tech. Report 1157.

[4] M.A. Fischler and R.C. Bolles. Random sample consensus: A paradigm for model fitting with applications to image analysis and automated cartography. *Communications of the ACM*, 24(6):381–395, 1981. Also in Readings in Computer vision, ed. Fischler.

[5] R.I. Hartley. Estimation of relative camera positions for uncalibrated cameras. In *Proc. European Conference on Computer Vision*, pages 579–587, 1992.

[6] R.I. Hartley. Cheirality invariants. In *Proc. DARPA Image Understanding Workshop*, pages 745–753, U. of Maryland, 1993.

[7] R.I. Hartley. In defence of the 8-point algorithm. In *Proc. International Conference on Computer Vision*, pages 1064–1070, Cambridge, MA, 1995.

[8] O. Hesse. Die cubische Gleichung, von welcher die Lösung des Pro blems der Homographie von M. Chasles abhängt. *J. reine angew. Math.*, 62:188–192, 1863.

[9] T.S. Huang and O.D. Faugeras. Some properties of the E-matrix in two view motion estimation. *IEEE Transactions on Pattern Analysis and Machine Intelligence*, 11:1310–1312, 1989.

[10] H.C. Longuet-Higgins. A Computer Algorithm for Reconstructing a Scene from Two Projections. *Nature*, 293:133–135, 1981.

[11] Q.-T. Luong. *Matrice fondamentale et auto-calibration en vision par ordinateur*. PhD thesis, Universite de Paris-Sud, Orsay, Dec. 1992.

[12] Q.-T. Luong, R. Deriche, O.D. Faugeras, and T. Papadopoulo. On determining the Fundamental matrix: analysis of different methods and experimental results. Technical Report RR-1894, INRIA, 1993.

[13] Q.-T. Luong and O.D. Faugeras. A stability analysis of the fundamental matrix. In *Proc. European Conference on Computer Vision*, pages 577–588, Stockholm, Sweden, 1994.

[14] Q.-T. Luong and O.D. Faugeras. The fundamental matrix: theory, algorithms, and stability analysis. *Intl. Journal of Computer Vision*, 17(1):43–76, 1996.

[15] Q.-T. Luong and T. Viéville. Canonical representations for the geometries of multiple projective views. *Computer Visio and Image Understanding*, 64(2):193–229, 1996.

[16] S.J. Maybank. Properties of essential matrices. *International journal of imaging systems and technology*, 2:380–384, 1990.

[17] S.J. Maybank. *Theory of reconstruction from image motion*. Springer-Verlag, 1993.

[18] S.J. Maybank and O.D. Faugeras. A Theory of Self-Calibration of a Moving Camera. *The International Journal of Computer Vision*, 8(2):123–151, 1992.

[19] J. L. Mundy and A. Zisserman, editors. *Geometric invariance in computer vision*. MIT Press, 1992.

[20] S.I. Olsen. Epipolar line estimation. In *Proc. European Conference on Computer Vision*, pages 307–311, 1992.

[21] L. Quan. Invariants of 6 points from 3 uncalibrated images. Technical Report RT 101 IMAG - 19, LIFIA, Oct 1993.

[22] L. Robert. *Reconstruction de courbes et de surfaces par vision stéréoscopique. Applications a la robotique mobile*. PhD thesis, Ecole Polytechnique, 1993.

[23] L. Robert and O.D. Faugeras. Relative 3D Positioning and 3D Convex Hull Computation from a Weakly Calibrated Stereo Pair. In *Proc. International Conference on Computer Vision*, pages 540–543, Berlin, Germany, May 1993.

[24] Rudolf Sturm. Das Problem der Projektivität und seine Anwendung auf die Flächen zweiten Grades. *Math. Ann.*, 1:533–574, 1869.

[25] P.H.S. Torr and D.W. Murray. Outlier detection and motion segmentation. Technical Report OUEL 1987/93, Oxford University, September 1993.